Polymer Microspheres

International Edition: DOI: 10.1002/anie.201606283
German Edition: DOI: 10.1002/ange.201606283

Polymer and Mesoporous Silica Microspheres with Chiral Nematic Order from Cellulose Nanocrystals

*Pei-Xi Wang, Wadood Y. Hamad, and Mark J. MacLachlan**

Abstract: *Polymer microspheres with chiral nematic order were obtained from an emulsion polymerization technique using cellulose nanocrystals (CNCs) as the template. The growth of the liquid crystals from tiny tactoids to droplets with spherical symmetry was captured and investigated by both optical and electron microscopy for the first time. The size of the microspheres could be tuned between tens and hundreds of micrometers; to obtain single, integrated chiral nematic kernels, the size of water droplets in the emulsion should be similar to that of CNC tactoids. Through a double-matrix templating method, novel silica microspheres with chiral nematic order were fabricated, which showed a high surface area and mesoporosity. The methods developed here may help to reveal the evolution of other self-assembling systems, and these materials have potential applications in optical devices and chiral separations.*

Nematic and cholesteric (chiral nematic) liquid crystals confined to microdroplets or microspheres are of great interest for potential applications in displays, sensing, optofluidics, and optical devices.[1] Furthermore, the structures and topologies of these colloidal particles are scientifically very interesting.[2] For instance, when cholesteric liquid crystals are incorporated into microspheres, the resulting particles are chiral and may have appealing chiroptical properties. Both molecular and polymeric cholesteric liquid crystals have been formed into microspheres that have potential applications as microlasers and in photonics.[3] Aßhoff et al. recently showed that superstructures of photoresponsive chiral nematic microspheres prepared in a microfluidic device are promising for chiroptical switches and distributors.[4] Despite growing interest in solid chiral particles, there are still few examples of these materials.[5]

As an inexpensive, sustainable nanomaterial that can be easily extracted from our forests and fields, cellulose nanocrystals (CNCs) have attracted widespread interest in recent years for their optical, mechanical, and electromagnetic properties that are being exploited for a variety of applications.[6] Above a critical concentration, aqueous suspensions of CNCs spontaneously form a chiral nematic (cholesteric) liquid-crystalline phase,[7] which has been applied for templating silica,[8] carbon,[9] and polymers[10] with long-range chiral nematic structures. Typically, CNCs dispersed in water or other solvents are mixed with the precursors of silica or polymers and, after an evaporation-induced self-assembly (EISA) process, composite materials with chiral nematic order are obtained.[11] However, such approaches only provide thin films that could be easily fractured by mechanical stress. Although this form may be useful in fields such as sensing,[12] gas chromatography,[13] and patterning,[14] and although efforts have been made to improve the properties of films,[15] many applications, such as HPLC and drug delivery, require microspheres with relatively uniform diameters.[16] To date, it has not been possible to make uniform and robust microbeads with chiral nematic structures from CNCs. Jativa et al. investigated the self-assembly of CNCs in water droplets,[17] but the chiral nematic order was not retained in the dried beads.

We recently studied the development of the chiral nematic phase of CNCs by polarized optical microscopy (POM) and monitored the formation and growth of CNC tactoids.[18] CNC tactoids are anisotropic microdroplets (10 to 100 μm in diameter) showing periodic birefringent bands that are about 10 μm apart (Supporting Information, Figure S1). They are nucleated from the isotropic phase and grow to form the long-range chiral nematic phase. As it has been demonstrated that the nonionic precursors of polyacrylamide (PAAm) hydrogels are compatible with the self-organization of CNCs in water,[19] we hypothesized that the polymerization of PAAm in inverse emulsions could be used to capture the chiral nematic structure of CNCs in microspheres. CNC tactoids would first form in tiny water droplets of an inverse emulsion system in the presence of PAAm precursors, then photopolymerization to PAAm would solidify these droplets with the chiral nematic tactoids encapsulated. Here we demonstrate the successful formation of PAAm/CNC microspheres with chiral nematic structures. The size of the microspheres can be tuned between tens and hundreds of micrometers. Mesoporous silica microspheres with chiral nematic order were also fabricated through a double-matrix method. These novel polymer and silica microspheres with chiral nematic structures may offer new opportunities for HPLC and other applications. As well, they open a new window to watch the evolution of a chiral nematic liquid crystal in a confined space.

CNCs used in this work are obtained by hydrolysis of wood pulp with sulfuric acid and are about 10–30 nm wide and about 100–400 nm long (Supporting Information, Figure S2). Figure 1 a depicts the process used to make polymer micro-

[*] P.-X. Wang, Prof. M. J. MacLachlan
Department of Chemistry, University of British Columbia
2036 Main Mall, Vancouver, British Columbia, V6T 1Z1 (Canada)
E-mail: mmaclach@chem.ubc.ca
Dr. W. Y. Hamad
FPInnovations
2665 East Mall, Vancouver, British Columbia, V6T 1Z4 (Canada)
Supporting information and the ORCID identification number(s) for the author(s) of this article can be found under: http://dx.doi.org/10.1002/anie.201606283.

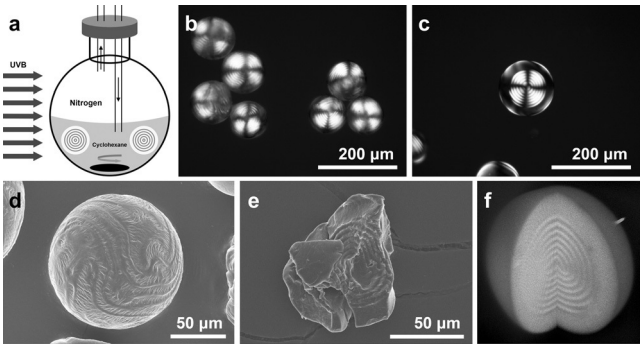

Figure 1. a) Cartoon depiction of the inverse emulsion photopolymerization system. b) POM image of dried microbeads. c) POM image of microbeads after swelling in water. d) SEM image of a dried microbead. e) SEM image of a broken microbead cracked in liquid nitrogen. f) 3D reconstructed confocal fluorescence microscopy image of a microgel showing the multi-shell spherical structure of the CNC periodic bands. The sample was stained by immersing the microsphere in a 0.1 wt% Rhodamine B aqueous solution before imaging. The sphere is 154 μm in diameter and 118 μm in height (orthogonal views are shown in the Supporting Information, Figure S5).

spheres with a chiral nematic arrangement of CNCs. In a standard procedure, a 4 wt% CNC suspension was mixed with acrylamide, a crosslinker, and a photoinitiator by sonication, then emulsified under nitrogen protection in cyclohexane (1:10 v/v) facilitated by Span-80 (0.8% w/v) and moderate stirring (400 rpm) to give micrometer-sized liquid microspheres. CNC tactoids were allowed to grow in these droplets for 9 h with the system sealed, then photopolymerization was initiated by UV irradiation to capture the tactoids inside PAAm microspheres. After removal of solvents, PAAm/CNC composite microbeads with chiral nematic order were obtained. The beads prepared this way have an average diameter of 125 μm (named as CAMB-M, Table 1).

Table 1: Processing parameters and average diameter of the PAAm/CNC microbeads.

Sample name	Cyclohexane [mL]	Span-80 [g]	CNC suspension [mL]	Stirring speed [rpm]	Mean diameter [μm]
CAMB-M	80	0.6	6.0	400	125
CAMB-S	80	1.2	6.0	600	30
CAMB-L	80	0.4	6.0	300	220

The as-prepared PAAm/CNC composite microbeads initially dried from ethanol are white and opaque, but transparent and colorless microbeads could be obtained by redispersing them in water then drying again under ambient conditions (Supporting Information, Figure S3a,c).[20] Chiral nematic tactoids of CNCs in these microbeads could be observed by POM under crossed polarizers (Figure 1b; Supporting Information, Figure S3b,d). They showed concentric retardation lines with a periodic spacing of about 5 μm (Figure 1b), indicating radially oriented helical axes.[3b,21] This texture is reminiscent of the ringed spherulitic textures observed for some molecular nematic liquid crystals and in a polypeptide.[22] Many of the spheres show a distinct Maltese cross pattern by POM, indicative of their spherical symmetry, suggesting that the helical axes of the liquid crystal are oriented along the radii. These microbeads can swell into transparent microgels in water owing to the hydrophilicity of PAAm, in which the periodic bands of the captured tactoids could be more clearly observed by POM under both crossed polarizers (Figure 1c; Supporting Information, Figure S4a,c) and reflected light (Supporting Information, Figure S4b,d). A scanning electron microscopy (SEM) image of a representative microbead (Figure 1d) shows the round shape typical of most of the beads, the pattern on its surface represents the turbulent flow of the liquid in the aqueous microdroplet during the polymerization process. Surface undulations on some microspheres with rather irregular shapes may arise from the inhomogeneity of the polymer matrices and sheer forces during the drying process, as these phenomena were not consistently observed on all of the spheres. After smashing some microbeads flash-frozen in liquid nitrogen with a hammer, we were able to directly observe the CNC tactoids in the center of the broken beads by SEM. A representative broken bead shown in Figure 1e has an onion-like structure that is consistent with the concentric circle patterns revealed by POM. The organization of CNC periodic bands in these microbeads can also be revealed by confocal laser scanning microscopy (CLSM) after staining the samples with a fluorescent dye (for example, rhodamine B) aqueous solution, as shown in Figure 1f and the Supporting Information, Figure S5. The contrast may arise from the uneven scattering of fluorescence owing to the optical anisotropy of the chiral nematic bands, rather than an uneven distribution of the dye. It is clear that the bands are arranged into a more-or-less spherical structure, while the overall organization of the bands is a spiral shape.

Because the helical pitch of the chiral nematic order in these microbeads is much larger than the wavelength of visible light, the chirality of these structures cannot be characterized with circular dichroism (CD) spectroscopy. Fortunately, the large size of CNC mesogens allows their orientations in the microbeads to be directly examined by electron microscopy. Although the beads can be briefly cracked in liquid nitrogen, frost immediately forms on the cold fracture surface, softens and smooths it after melting (Supporting Information, Figure S6). But, good-quality cross-sections could be obtained by smashing these microbeads after embedding them in epoxy resins (Supporting Information, Figure S7), and in this way we were able to clearly examine the organization of CNCs by SEM. The periodic bands of the captured tactoids often form a spiral structure with a disclination defect at the center rather than perfect concentric spherical shells (Figure 2a–c; Supporting Information, Figure S8). The left-handed chiral nematic order of CNCs is apparent at high magnification (Figure 2d–f). The orientation of CNCs is twisted 180 degrees between two adjacent bands, which means a half helical pitch. As indicated by POM observations, outside the tactoid is the isotropic region, in which CNCs are randomly arranged (Supporting Information, Figure S9). This phase separation phenomenon

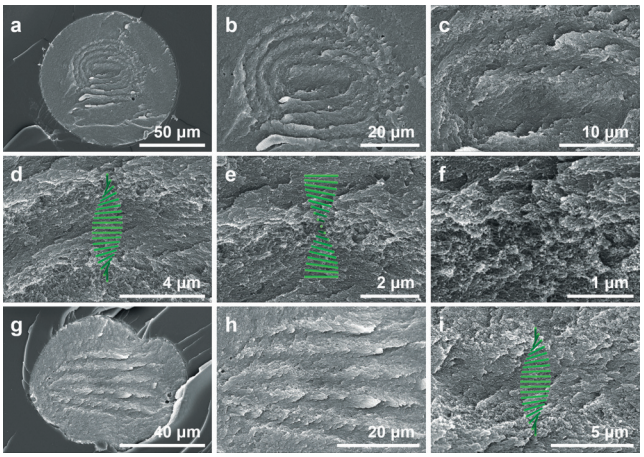

Figure 2. a) Cross-section SEM image for a microbead cracked after being embedded in epoxy resins. The CNC tactoid with a spiral structure is shown in (b) and (c). d)–f) Magnified SEM images for its left-handed chiral nematic bands. g) Cross-section SEM image for a microbead containing a tactoid with flat bands as shown in (h). A half helical pitch of this tactoid is indicated in (i).

is common in lyotropic liquid crystals. More SEM images showing spiral CNC chiral nematic bands can be found in the Supporting Information, Figure S10.

In some microbeads we also found tactoids having flat parallel periodic bands (Figure 2 g–i; Supporting Information, Figure S11), which are similar to those formed in bulk CNC suspensions. Interestingly, tactoids with arc-shaped bands were also discovered in some microbeads, as shown in the SEM images in the Supporting Information, Figure S12. We believe that these structures represent different stages of the growth of tactoids in aqueous microdroplets in inverse emulsions. Initially, a newly formed CNC tactoid in the center of a water droplet has flat periodic bands before its edge reaches the water–oil interface (Figure 3 a). The size of this tactoid gradually increases over time, accompanied by the generation of new bands, and eventually its growth is constrained by the boundary of the water droplet. The periodic bands then bend to fit the spherical shape of the water–oil interface (in this process an $S = +1/2$ disclination is generated), they keep extending along the interface or an outer adjacent band (Figure 3 b,c), and finally a concentric spherical multi-shell structure (in an ideal situation) or a spiraling structure (Figure 3 d) would be formed.

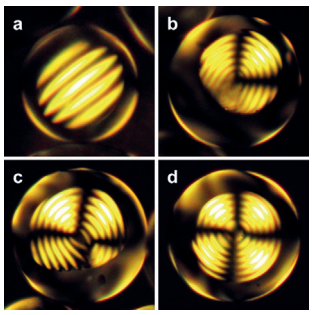

Figure 3. POM images of microgels showing CNC tactoids captured at different growth stages. From (a) to (d), the diameter of the microgel is 69 μm, 136 μm, 142 μm, and 141 μm, respectively.

We also monitored the growth process of tactoids in emulsions as a function of time. Samples were taken from the emulsion at 30 min intervals and examined by POM. Many small tactoids (with two or three bands) appear soon after the injection of the CNC aqueous suspension into cyclohexane. A newly formed tactoid in a water droplet that was sampled 30 min after emulsification is shown in the Supporting Information, Figure S13a. More tactoids are generated over time and their coexistence in the same droplet could be observed (Figure S13b). Bigger tactoids can be formed through a coalescence mechanism (Figure S13c) as confirmed by real-time POM monitoring of bulk CNC suspensions;[18] other growth mechanisms are likely also simultaneously active. The growth seemed to be slow as water evaporation was prohibited, thus keeping the CNC concentration low. Bent bands were observed when the tactoids are large enough to be influenced by the water–oil interface (Figure S13d). Large CNC tactoids showing concentric retardation lines by POM are prevalent about 9 h after emulsification (Figure S13e); they keep growing and finally occupy most of the space in the water droplets (Figure S13f).

Although the spherical confinement of cholesteric liquid crystals has been extensively studied,[3b,21] in most cases only thermotropic liquid crystals were used, which are molecular substances that can self-assemble into chiral nematic structures very quickly. As large rod-like particles, CNCs have much slower dynamics. Thus, the evolution of liquid crystallinity in CNC suspensions can take many hours, providing a good opportunity to study the formation of a chiral nematic phase in a confined space starting from an isotropic dispersion. In this work we have observed that the chiral nematic bands of a CNC tactoid in a microdroplet grow along the water–oil interface, but there are many issues for further study.

The average diameter of the microbeads can be easily controlled from 30 to 220 μm by changing the amount of surfactant and stirring speed used. A larger amount of surfactant and a higher stirring speed afforded smaller microbeads, as verified by SEM measurements (Figure 4; Table 1; Supporting Information, Figure S14). After swelling into microgels in water, the existence of CNC tactoids inside could be clearly observed by POM (Figure 4 a–c).

Not surprisingly, although most of the tiny microbeads (about 30 μm, named as CAMB-S) show chiral nematic tactoids with concentric spherulitic patterns, in general they only have one or two retardation lines. On the other hand, CNC tactoids in large microbeads (about 220 μm, named as CAMB-L) were not efficiently integrated due to the rather long distances between them; thus, the multiple tactoids were not forced to merge into a single one. These results confirmed our hypothesis that CNC tactoids would be better formed in water droplets with comparable sizes to the individual tactoids.

With these results, we further expanded this inverse emulsion method to the fabrication of mesoporous silica microspheres with chiral nematic order. In a typical procedure, an acidic CNC suspension was mixed with PAAm precursors (acrylamide, a crosslinker, and a photoinitiator) and tetramethyl orthosilicate (TMOS), then homogenized by

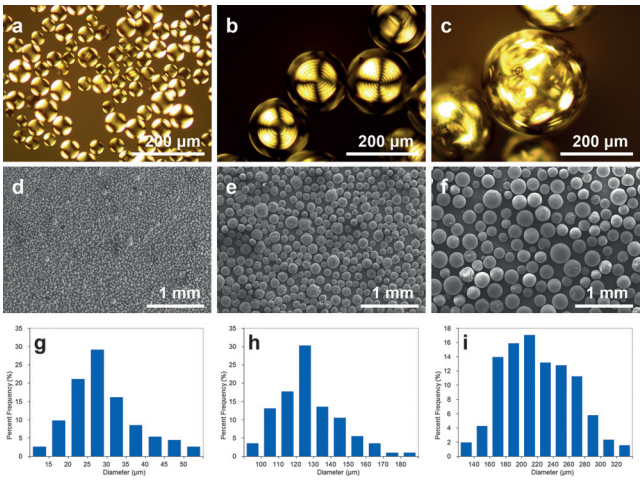

Figure 4. a)–c) POM images for CAMB-S, CAMB-M, and CAMB-L microbeads, respectively, after swelling in water. d)–f) SEM images for dried CAMB-S, CAMB-M, and CAMB-L microbeads. g)–i) Size distribution histograms for dried CAMB-S, CAMB-M, and CAMB-L microbeads based on SEM measurements.

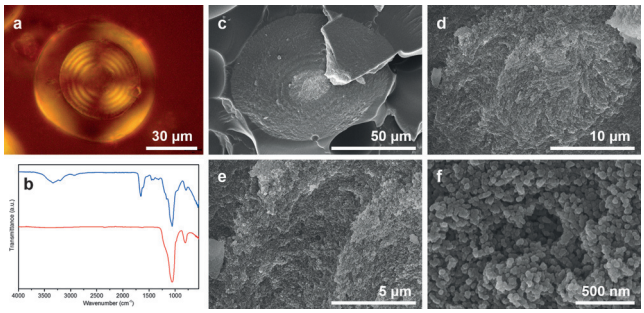

Figure 5. a) POM image for mesoporous silica microspheres with chiral nematic order. b) FTIR spectra for CNC/PAAm/silica composite microspheres (upper blue curve) and silica microspheres (lower red curve). c) SEM image showing the concentric circle pattern at the cross-section of a silica microsphere. d) Central region of this microsphere. e) A half helical pitch of the chiral nematic order. f) High-magnification image showing the silica nanoparticles in this microsphere.

sonication and used as the aqueous phase. Other experimental conditions were kept the same as those used for the preparation of CAMB-M samples. TMOS underwent a sol–gel transition in the acidic environment during the growth of CNC tactoids in the aqueous microdroplets. After an appropriate period of time, photopolymerization was initiated by UV irradiation, and a crosslinked polyacrylamide matrix was formed to capture the chiral nematic order of CNC tactoids in solid microspheres. An ethanolic solution of ammonia was then added to accelerate the condensation of silanol groups of the silica gels inside the microspheres, thus forming an additional matrix of silica to support the chiral nematic structures (a double-matrix method). After complete drying, the microspheres were calcined at 540 °C in air to remove all the organics including CNCs and PAAm, yielding mesoporous silica microspheres with chiral nematic order.

The chiral nematic structures in CNC/PAAm/silica composite microspheres were characterized with SEM (Supporting Information, Figure S15). After calcination, the periodically spaced bands from CNC tactoids perfectly remained in many of the silica microspheres, which could be observed with POM (Figure 5a; Supporting Information, Figure S16). The complete removal of cellulose nanocrystals, polyacrylamide and other organic compounds was confirmed by FTIR spectroscopy and elemental analysis. IR spectra (Figure 5b) of CNC/PAAm/silica composite microbeads showed characteristic peaks of cellulose (1161 cm^{-1} for pyranose rings; 3339 cm^{-1} for hydroxy groups) and polyacrylamide (1656 cm^{-1} for carbonyl groups; 1617 cm^{-1} for amino groups; 1450 cm^{-1} for methylene bridges), but after calcination, only the typical stretching vibration bands of silica networks remained (1056 cm^{-1} and 806 cm^{-1} for Si-O-Si). Elemental analysis of composite microbeads gave 8.27 wt% nitrogen, 31.02 wt% carbon, and 5.26 wt.% hydrogen, while these three elements in the silica microspheres were all lower than the detection limit.

Cross-sections of the silica microspheres were obtained by breaking an epoxy resin with samples embedded inside, then the periodic bands (Figure 5c; Supporting Information, Figure S17a,b) and chiral nematic structures (Figure 5d,e; Supporting Information, Figure S17c,d) in these silica microspheres could be directly examined with SEM. The silica microspheres are composed of grain-shaped nanoparticles as shown in high magnification images (Figure 5f), while the cross-sections of composite microbeads exhibit a completely different appearance as the CNCs could be clearly observed as nanorods (Supporting Information, Figure S18). This morphological difference can also be seen at the surfaces of these microspheres before and after calcination (Supporting Information, Figure S19).

The mesoporous properties of these silica microspheres were confirmed by nitrogen adsorption and desorption measurements (Supporting Information, Figure S20). The sample showed a BET surface area of 257 $m^2 g^{-1}$, a BJH adsorption cumulative pore volume of 0.993 $cm^3 g^{-1}$, and a BJH adsorption average pore width of 14.6 nm. The coexistence of a high surface area, mesoporosity, good thermal stability, and chiral nematic order in these silica microspheres gives them potential applications in chiral separations.

In summary, we successfully captured the chiral nematic organization of CNCs in polymer microspheres by growing CNC tactoids in aqueous microdroplets of an inverse emulsion system. The chiral nematic structures of CNCs are perfectly preserved within the polymer matrix, as characterized by both optical and electron microscopy. The size of the microbeads can be adjusted by changing the stirring speed and the amount of surfactant used. Furthermore, we have found that to obtain single, integrated chiral nematic kernels with concentric spherical multi-shell structures, the size of water droplets in the inverse emulsion should be similar to that of CNC tactoids. We also expanded this method to the synthesis of silica microspheres with chiral nematic order, which exhibit a high surface area and mesoporosity. These microspheres should be scalable, and their high stability

makes them promising candidates for novel sensors, microlasers, micro-optical devices, and chiral separation materials.

Acknowledgements

We are grateful to NSERC for funding (Discovery Grant). P.X.W. thanks UBC for a 4YF Fellowship and Dr. Saeid Kamal (UBC LASIR Facility) for assistance with CLSM. We also thank FPInnovations and CelluForce for the donation of CNCs used in this work, and we acknowledge the assistance of the UBC Bioimaging Facility.

Keywords: cellulose nanocrystals · chiral nematic structure · liquid crystals · mesoporous silica · microspheres

How to cite: *Angew. Chem. Int. Ed.* **2016**, *55*, 12460–12464
Angew. Chem. **2016**, *128*, 12648–12652

[1] a) M. Humar, I. Muševič, *Opt. Express* **2011**, *19*, 19836–19844; b) Y. Uchida, Y. Iwai, T. Akita, K. Yamamoto, N. Nishiyama, *Mol. Cryst. Liq. Cryst.* **2015**, *613*, 82–87; c) Y. Iwai, H. Kaji, Y. Uchida, N. Nishiyama, *Mol. Cryst. Liq. Cryst.* **2015**, *615*, 9–13; d) S. S. Lee, B. Kim, S. K. Kim, J. C. Won, Y. H. Kim, S.-H. Kim, *Adv. Mater.* **2015**, *27*, 627–633.

[2] a) I. Muševič, *Philos. Trans. R. Soc. London Ser. A* **2013**, *371*, 20120266; b) I. Muševič, *Liq. Cryst.* **2014**, *41*, 418–429.

[3] a) S. S. Lee, S. K. Kim, J. C. Won, Y. H. Kim, S.-H. Kim, *Angew. Chem. Int. Ed.* **2015**, *54*, 15266–15270; *Angew. Chem.* **2015**, *127*, 15481–15485; b) M. Humar, I. Muševič, *Opt. Express* **2010**, *18*, 26995–27003.

[4] S. J. Aßhoff, S. Sukas, T. Yamaguchi, C. A. Hommersom, S. Le Gac, N. Katsonis, *Sci. Rep.* **2015**, *5*, 14183.

[5] a) G. Cipparrone, A. Mazzulla, A. Pane, R. J. Hernandez, R. Bartolino, *Adv. Mater.* **2011**, *23*, 5773–5778; b) E. Beltran-Gracia, O. L. Parri, *J. Mater. Chem. C* **2015**, *3*, 11335–11340.

[6] a) Y. Habibi, L. A. Lucia, O. J. Rojas, *Chem. Rev.* **2010**, *110*, 3479–3500; b) "Sustainable Production of Fuels, Chemicals, and Fibers from Forest Biomass": W. Y. Hamad, *ACS Symposium Series*, *Vol. 1067* (Eds.: J. Y. Zhu, X. Zhang, X. J. Pan), American Chemical Society, Washington, DC, **2011**, pp. 301–321; c) R. J. Moon, A. Martini, J. Nairn, J. Simonsen, J. Youngblood, *Chem. Soc. Rev.* **2011**, *40*, 3941–3994; d) D. Klemm, F. Kramer, S. Moritz, T. Lindström, M. Ankerfors, D. Gray, A. Dorris, *Angew. Chem. Int. Ed.* **2011**, *50*, 5438–5466; *Angew. Chem.* **2011**, *123*, 5550–5580.

[7] a) R. H. Marchessault, F. F. Morehead, N. M. Walter, *Nature* **1959**, *184*, 632–633; b) J.-F. Revol, H. Bradford, J. Giasson, R. H. Marchessault, D. G. Gray, *Int. J. Biol. Macromol.* **1992**, *14*, 170–172.

[8] K. E. Shopsowitz, H. Qi, W. Y. Hamad, M. J. MacLachlan, *Nature* **2010**, *468*, 422–425.

[9] K. E. Shopsowitz, W. Y. Hamad, M. J. MacLachlan, *Angew. Chem. Int. Ed.* **2011**, *50*, 10991–10995; *Angew. Chem.* **2011**, *123*, 11183–11187.

[10] M. K. Khan, M. Giese, M. Yu, J. A. Kelly, W. Y. Hamad, M. J. MacLachlan, *Angew. Chem. Int. Ed.* **2013**, *52*, 8921–8924; *Angew. Chem.* **2013**, *125*, 9089–9092.

[11] J. A. Kelly, M. Giese, K. E. Shopsowitz, W. Y. Hamad, M. J. MacLachlan, *Acc. Chem. Res.* **2014**, *47*, 1088–1096.

[12] M. Giese, L. K. Blusch, M. K. Khan, W. Y. Hamad, M. J. MacLachlan, *Angew. Chem. Int. Ed.* **2014**, *53*, 8880–8884; *Angew. Chem.* **2014**, *126*, 9026–9030.

[13] J.-H. Zhang, S.-M. Xie, M. Zhang, M. Zi, P.-G. He, L.-M. Yuan, *Anal. Chem.* **2014**, *86*, 9595–9602.

[14] M. K. Khan, A. Bsoul, K. Walus, W. Y. Hamad, M. J. MacLachlan, *Angew. Chem. Int. Ed.* **2015**, *54*, 4304–4308; *Angew. Chem.* **2015**, *127*, 4378–4382.

[15] a) J. H. Park, J. Noh, C. Schütz, G. Salazar-Alvarez, G. Scalia, L. Bergström, J. P. F. Lagerwall, *ChemPhysChem* **2014**, *15*, 1477–1484; b) B. Zhu, R. Merindol, A. J. Benitez, B. Wang, A. Walther, *ACS Appl. Mater. Interfaces* **2016**, *8*, 11031–11040.

[16] H. Kawaguchi, *Prog. Polym. Sci.* **2000**, *25*, 1171–1210.

[17] F. Jativa, C. Schütz, L. Bergström, X. Zhang, B. Wicklein, *Soft Matter* **2015**, *11*, 5374–5380.

[18] P.-X. Wang, W. Y. Hamad, M. J. MacLachlan, *Nat. Commun.* **2016**, *7*, 11515.

[19] J. A. Kelly, A. M. Shukaliak, C. C. Y. Cheung, K. E. Shopsowitz, W. Y. Hamad, M. J. MacLachlan, *Angew. Chem. Int. Ed.* **2013**, *52*, 8912–8916; *Angew. Chem.* **2013**, *125*, 9080–9084.

[20] The transparent and colorless microbeads, prepared by redispersing the original samples in water and drying again, were only used to obtain the POM images shown in Figure 1b and the Supporting Information, Figure S3, while other POM images and all of the SEM images in this work were obtained with the original as-prepared microspheres.

[21] a) D. Seč, T. Porenta, M. Ravnik, S. Žumer, *Soft Matter* **2012**, *8*, 11982–11988; b) G. Tkachenko, E. Brasselet, *Nat. Commun.* **2014**, *5*, 3577.

[22] a) C. Robinson, *Trans. Faraday Soc.* **1956**, *52*, 571–592; b) A. C. Sparavigna, *Phase Transitions* **2009**, *82*, 620–631.

Received: June 28, 2016
Revised: July 25, 2016
Published online: September 1, 2016

